In-Plane Tow Deformations Due to Steering in Automated Fiber Placement

Roudy Wehbe,[1] Ramy Harik,[2] and Zafer Gürdal[3]
University of South Carolina, Columbia, SC, 29201

Automated fiber is placement (AFP) is an additive manufacturing process used to fabricate composite structures for aerospace applications. During the AFP process, fiber steering is needed to manufacture curved-shell structures, or to manufacture variable stiffness plates. Due to steering, the carbon fiber tows undergo several deformation mechanisms which are classified in this paper as strain deformations, in-plane defamations (waviness and bunching) and out-of-plane deformations (wrinkling and folding). The aim of this work is to understand the in-plane deformation mechanisms that might appear during the AFP process. To do so, an approach is presented based on the physics of a constrained path that predicts which of the proposed mechanisms is predominant from an energy standpoint. A numerical scheme is implemented to obtain the final shape of the deformed tow based on the steering conditions as well as other relevant material properties and process parameters. Here only in-plane deformations are considered in the formulation; hence the differential length due to steering is absorbed by fiber waviness or compressive strains on the compressive side of the tow, and fiber straightening/bunching or tensile strains on the tensile side. The importance of the stiffness of the foundation and the steering radius on the final deformed shape of the tow is also discussed.

I. Nomenclature

A. Latin Symbols

A	=	cross-sectional area
A_{ij}	=	components of the extensional stiffness matrix
$\boldsymbol{C}$, $\boldsymbol{C_p}$	=	curve representing the centerline of the tow-path, curve parallel to the centerline
D_{ij}	=	components of the bending stiffness matrix
d	=	distance from the neutral axis
E_{11}, E_{22}	=	modulus of elasticity along the fiber and orthogonal to the fiber's direction respectively
$\boldsymbol{F}$	=	force vector
$\mathcal{F}$	=	Euler-Lagrange functional
$\boldsymbol{G}$	=	error vector function
f_x, f_y	=	forces in the x and y-direction
H	=	tow thickness
I	=	moment of inertia
J	=	Jacobian matrix
K	=	energy stored in elastic foundation
k_x, k_y	=	elastic modulus of the foundation in the x and y-direction
L	=	length of the tow
l'	=	strain along the length
r	=	direction perpendicular to the fiber path
s	=	direction along the fiber path
U	=	elastic strain energy
u	=	displacement in the x-direction

[1] PhD Candidate, Mechanical Engineering Department, AIAA Student Member.
[2] Associate Professor, Mechanical Engineering Department.
[3] Professor, , Mechanical Engineering Department, Lifetime Member and Associate Fellow.

v = displacement in the y-direction
w = tow width
W = work done by the forces

B. Greek symbols

γ = in-plane rotation angle
$\boldsymbol{\Delta}$ = total displacement vector
δ = finite difference step
ϵ^o = mid-plain strain
κ^o = mid-plane curvature
ν_{12} = Poisson's ratio
Π = total energy
ρ = radius of curvature

II. Introduction

Automated Fiber placement (AFP) is gaining advantage over hand layup processes due to improvements in productivity, and over automated tape laying due to the possibility of manufacturing complex shapes and producing steered fiber laminates. However, tow steering in AFP is limited due to potential defects that occur during the manufacturing process such as wrinkling and folding. These defects are mainly due to the mismatch in length between the straight tow delivered from the machine head and the curved path on the mold surface along the edges of the path. To absorb this difference in length, several mechanisms are proposed in this paper, and classified as follows: (a) strain deformations such as tensile, compressive, and shear which are uniform along the length, (b) localized in-plane deformations such as in-plane waviness and tow straightening/bunching, and (c) localized out-of-plane deformations such as wrinkling and folding (see Fig. 1 and Fig. 2). The presence of such defects in the manufactured composite part might lead to property degradation resulting in weaker parts than designed.

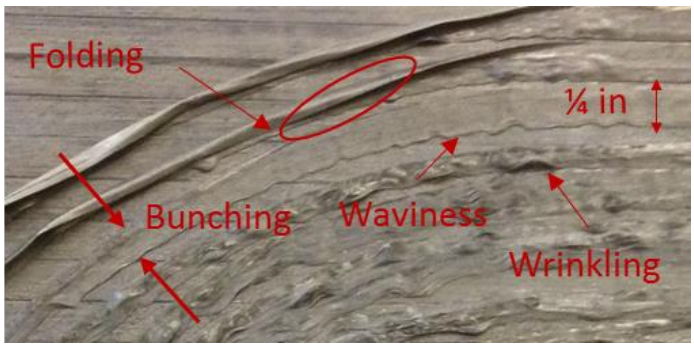

Fig. 1: Tow deformations due to excessive steering (Courtesy of Mc*Nair* Center, University of South Carolina)

Common defects observed due to steering are reported in the literature to be tow buckling (wrinkling), tow pull up (folding), and tow misalignment [1] (in-plane deformations). Efforts to model tow wrinkling in AFP are reported for the case of thermoset [2] and dry fiber [3] tows. The limitation of these models is their incapability to capture defects that occur on the tensile side of the tow such as folding or fiber bunching, and it is difficult to apply these models for the case of tows laid on general surfaces. Another model to predict wrinkling that extends to general surfaces was presented by the authors based on the geometry of the tow-path [4, 5]. As for the case of modeling in-plane deformations due to steering, fiber waviness was investigated as a possible mechanism on the compressive edge of the tow [6]. However, the deformed shape was assumed to be sinusoidal, and the corresponding amplitude and wavelength were determined statistically from experiments. To the authors' knowledge, there is no effort reported in the literature related to modeling or understanding the occurrence of fiber bunching/straightening on the tensile side of the tow.

In this paper, the carbon fiber tow used in the AFP process is modeled as several fiber bundles laying on a stiff foundation. The total energy of the system is derived for the case of small strains and large rotations. Detailed derivations and other assumptions are shown in Section III. The numerical solution approach to solve the governing equations is discussed in Section IV. The results for a tow placed on a constant curvature path are shown in section V

along with an investigation of the effect of the stiff foundation and the steering radius. Finally, conclusion, recommendations and future work are discussed in Section VI.

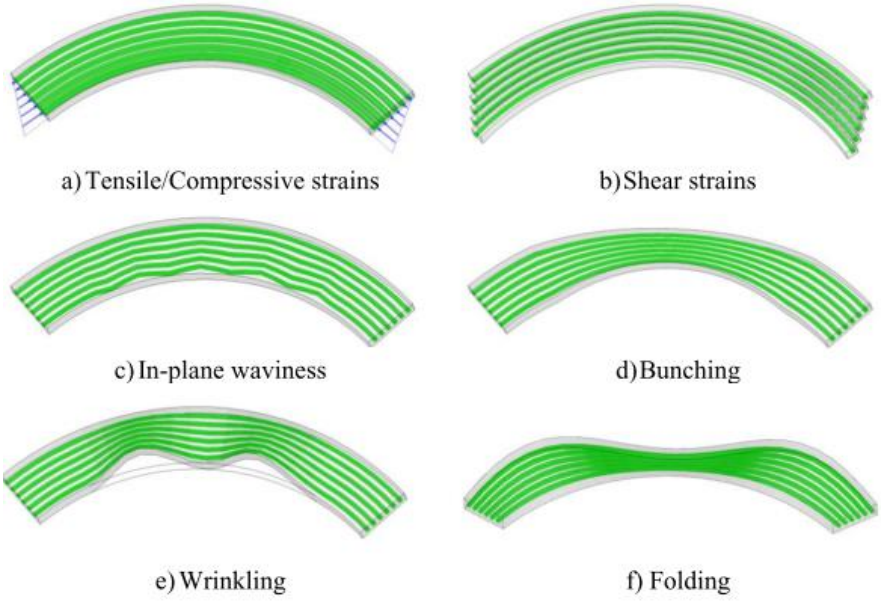

Fig. 2: Deformation mechanisms for differential length absorption[4]

III. Governing Equations

During the AFP process, the machine head by the means of the roller forces the tow to adhere to a substrate following a prescribed path. Hence, the problem here is formulated in a way that the boundary of the tow satisfies a specific displacement field imposed by the roller due to steering. The thin tow is considered as several fiber bundles laying on a stiff foundation. A single bundle is shown in Fig. 3.

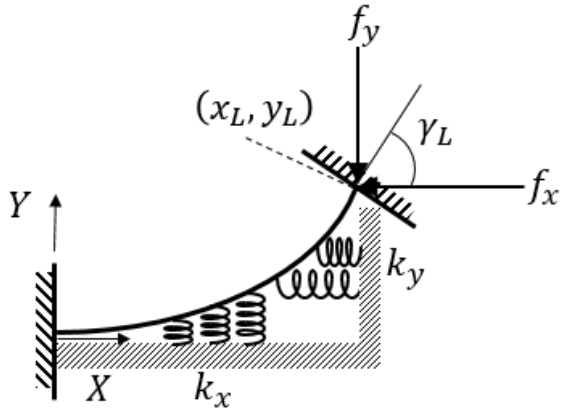

Fig. 3: Schematic of a tow during AFP

The total energy Π of the system shown in Fig. 3 can be expressed as:

$$\Pi = U - W + K\,, \tag{1}$$

where U is the elastic strain energy, K is the energy stored in the elastic foundation, and W is the work generated by the applied forces necessary to satisfy the boundary conditions. The strain energy U of a thin composite laminate structure can be expressed as [7]:

$$U = \frac{1}{2}\iint \left[A_{11}{\epsilon_s^o}^2 + 2A_{12}\epsilon_s^o\epsilon_r^o + A_{22}{\epsilon_r^o}^2 + A_{66}{\gamma_{sr}^o}^2 + D_{11}{\kappa_s^o}^2 + 2D_{12}\kappa_s^o\kappa_r^o + D_{22}{\kappa_r^o}^2 + D_{66}{\kappa_{sr}^o}^2\right] ds dr, \tag{2}$$

where s and r represent the directions along and perpendicular to the path, respectively, ϵ^o and κ^o are the mid-plane strains and curvatures, and A_{ij} and D_{ij} are components of the extensional and bending stiffness matrices. In the first step of the in-plane tow deformations modeling the tow is restricted to deform in-plane only, hence out-of-plane terms in the elastic strain energy equation are dropped. In addition, the fiber bundle is assumed to be very stiff in the longitudinal direction, whereas the stiffness in the transverse and shear directions are mainly governed by the uncured resin. In a way, the tow is highly anisotropic, and the A_{12}, A_{22}, and A_{66} terms are orders of magnitude smaller in comparison to A_{11}. Therefore, ϵ_s^o will be the first term investigated for the case where the strains are small, but large rotations are applied. Hence, ϵ_s^o has the form of:

$$\epsilon_s^o = l'(s) - r\,\kappa_r^o(s)\,, \tag{3}$$

where $l'(s)$ is the change in length along the fiber direction, and $\kappa_r^o(s) = \gamma'(s)$ is the in-plane curvature due to the fiber's rotation. From classical lamination theory, and using Kirchhoff-Love assumptions, the components of the stiffness matrix A_{ij} are obtained from:

$$A_{ij} = \sum_{k=1}^{n} \{Q_{ij}\}_n (z_k - z_{k-1}) \tag{4}$$

For the case of a single layer tow $n = 1$, $z_0 = -H/2$ and $z_1 = H/2$ with H being the thickness of the tow, the A_{11} term becomes:

$$A_{11} = Q_{11}H, \tag{5}$$

with:

$$Q_{11} = \frac{E_{11}^2}{E_{11} - \nu_{12}^2 E_{22}} \cong E_{11}, \tag{6}$$

since the modulus in the transverse direction E_{22} is order of magnitudes smaller than the modulus in the longitudinal direction E_{11} for an uncured thermoset prepreg tow. Therefore, the strain energy can be expressed as:

$$U = \frac{1}{2}\int_0^L \int_{-\frac{w}{2}}^{\frac{w}{2}} A_{11}\,{\epsilon_s^o}^2\, dr\, ds = \frac{1}{2}\int_0^L E_{11}\left(A\,{l'}^2(s) + I\,{\gamma'}^2(s)\right) ds\,, \tag{7}$$

with $A = H\,w$ being the cross-sectional area of the tow, and $I = (H\,w^3)/12$ its moment of inertia.

The total work W generated by the applied forces $\boldsymbol{F} = \{f_x, f_y\}$ can be expressed as:

$$W = \boldsymbol{F}\cdot\boldsymbol{\Delta}\,, \tag{8}$$

with $\boldsymbol{\Delta} = \{(x_L - x_0) - L, (y_L - y_0) - 0\}$ being the total displacement vector. The relationship between differential lines in the x and y-directions (dx and dy), strain, arc-length, and rotation is shown in Fig. 4, and can be expressed as:

$$dx = (ds + dl)\cos\gamma = \left(1 + \frac{dl}{ds}\right)\cos\gamma\ ds\,, \tag{9}$$

$$dy = (ds + dl)\sin\gamma = \left(1 + \frac{dl}{ds}\right)\sin\gamma\ ds\,. \tag{10}$$

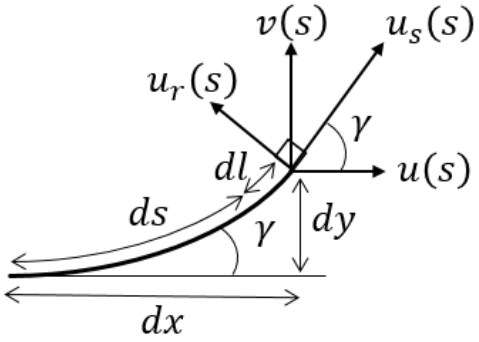

Fig. 4: Strain-rotation relationship and displacement components

Integrating both sides of equations (9) and (10) between 0 and a total length L, it can be shown that:

$$x_L - x_0 = \int_0^L (1 + l') \cos\gamma \; ds \,, \tag{11}$$

$$y_L - y_0 = \int_0^L (1 + l') \sin\gamma \; ds \,. \tag{12}$$

Replacing equations (11) and (12) into equation (8), the total amount of work required at equilibrium can be obtained as follows:

$$W = f_x \left[\int_0^L (1 + l') \cos\gamma \; ds - L \right] + f_y \int_0^L (1 + l') \sin\gamma \; ds \,. \tag{13}$$

Lastly, the energy term resulting from the elastic foundation can be expressed as:

$$K = \frac{1}{2} \int_0^L k_x \, u^2(s) \, ds + \frac{1}{2} \int_0^L k_y \, v^2(s) \, ds \,, \tag{14}$$

where, k_x and k_y are the modulus of the foundation in the x and y direction respectively and having the dimension of a force divided by the square of a length [8]. Here, $u(s)$ and $v(s)$ refer to the displacement in the x and y directions respectively, and are expressed as:

$$u(s) = x(s) - x_{ref}(s), \tag{15}$$

$$v(s) = y(s) - y_{ref}(s), \tag{16}$$

$x_{ref}(s)$ and $y_{ref}(s)$ are the reference coordinates of the initial undeformed tow. Hence the total potential energy of the deformed tow is expressed as:

$$\begin{aligned} \Pi = \frac{1}{2} \int_0^L (E_{11} A l'^2 + E_{11} I \gamma'^2) \, ds - f_x \left[\int_0^L (1 + l') \cos\gamma \; ds - L \right] - f_y \int_0^L (1 + l') \sin\gamma \; ds \\ + \frac{k_x}{2} \int_0^L u^2(s) \, ds + \frac{k_y}{2} \int_0^L v^2(s) \, ds \,. \end{aligned} \tag{17}$$

IV. Numerical Solution Approach

The total energy shown in equation (17) contains 4 unknown functions $\gamma(s)$, $l(s)$, $x(s)$, and $y(s)$, and 2 unknown constants f_x and f_y. Note that $x(s)$ and $y(s)$ can be expressed in terms of $\gamma(s)$ and $l(s)$ by integrating equations (9) and (10), hence, the functional Π can be expressed in terms of the first two functions only as:

$$\Pi\big(\gamma(s), l(s)\big) = \int_0^L \mathcal{F}\big(s, \gamma(s), \gamma'(s), l'(s)\big) \, ds \tag{18}$$

Using Euler-Lagrange principle to minimize the total energy Π, the following set of partial differential equations has to be satisfied:

$$\begin{cases} \dfrac{d}{ds}\left(\dfrac{\partial \mathcal{F}}{\partial \gamma'}\right) - \dfrac{\partial \mathcal{F}}{\partial \gamma} = 0 \\ \dfrac{d}{ds}\left(\dfrac{\partial \mathcal{F}}{\partial l'}\right) - \dfrac{\partial \mathcal{F}}{\partial l} = 0 \,. \end{cases} \tag{19}$$

By evaluating the partial derivatives in equation (19), and including the two additional equations relating $x(s)$ and $y(s)$ to $\gamma(s)$ and $l(s)$, the following system of differential equations can be obtained:

$$\boldsymbol{System}\big(f_x, f_y, s\big) = \begin{cases} E_{11} I \, \gamma'' - f_x (1 + l') \sin\gamma + f_y (1 + l') \cos\gamma + k_x u \, y - k_y v \, x = 0 \\ E_{11} A \, l' = F + f_x \cos\gamma + f_y \sin\gamma - k_x u \, x - k_y v \, y \\ x' = (1 + l') \cos\gamma \\ y' = (1 + l') \sin\gamma \end{cases} . \tag{20}$$

Equation (20) contains a 2nd order derivative of γ and 1st order derivatives for $l, x,$ and y. Hence, five boundary conditions are needed. The starting point of the path can provide four of them:

$$\text{At s} = 0\text{: } \gamma(0) = l(0) = x(0) = y(0) = 0 \,, \tag{21}$$

and the remaining boundary condition is obtained at the endpoint:

$$\text{At s} = \text{L: } \gamma(L) = \gamma_L. \tag{22}$$

The remaining unknowns in equation (20) are the forces f_x and f_y. These forces have to satisfy two remaining boundary conditions x_L and y_L; the coordinates of the endpoint of the fiber bundle enforced by the roller at s = L. To

accomplish that, an iterative approach is implemented as shown in Fig. 5. First, an initial value for the forces is assumed. A good starting point can be assumed as $f_{x_o} = f_{y_0} = 0$. Then, the system in (20) can be solved for these assumed values, and the functions $x(s)$ and $y(s)$ can be obtained. To ensure the boundary conditions are fulfilled, the following vector function providing two additional equations must be satisfied:

$$\boldsymbol{G}(f_x, f_y) = \begin{Bmatrix} x^*(f_x, f_y) - x_L \\ y^*(f_x, f_y) - y_L \end{Bmatrix} = \mathbf{0}\,, \tag{23}$$

where x^* and y^* are the values of $x(s)$ and $y(s)$ evaluated at s = L. Newton-Raphson method is applied to the system of equations in (23) iteratively to determine the forces f_x and f_y such that:

$$\begin{Bmatrix} f_{x_{n+1}} \\ f_{y_{n+1}} \end{Bmatrix} = \begin{Bmatrix} f_{x_n} \\ f_{y_n} \end{Bmatrix} - c\, J^{-1}\left(f_{x_n}, f_{y_n}\right)\, \boldsymbol{G}\left(f_{x_n}, f_{y_n}\right), \tag{24}$$

where $J\left(f_{x_n}, f_{y_n}\right)$ is the Jacobian matrix for the vector function $\boldsymbol{G}\left(f_{x_n}, f_{y_n}\right)$:

$$J = \left[\frac{\partial \boldsymbol{G}\left(f_{x_n}, f_{y_n}\right)}{\partial f_x} \quad \frac{\partial \boldsymbol{G}\left(f_{x_n}, f_{y_n}\right)}{\partial f_y}\right]. \tag{25}$$

Note that the vector function $\boldsymbol{G}(f_x, f_y)$ requires solving the system in (20) numerically then evaluating the numerical values of x^* and y^* at $s = L$. Therefore, the partial derivatives in the Jacobian matrix (25) cannot be evaluated analytically and a numerical method must be used. Here, a finite difference technique such as the central difference is used to approximate the numerical value of the Jacobian matrix:

$$J \cong \left[\frac{\boldsymbol{G}\left(f_{x_n} + \delta, f_{y_n}\right) - \boldsymbol{G}\left(f_{x_n} - \delta, f_{y_n}\right)}{2\delta} \quad \frac{\boldsymbol{G}\left(f_{x_n}, f_{y_n} + \delta\right) - \boldsymbol{G}\left(f_{x_n}, f_{y_n} - \delta\right)}{2\delta}\right]. \tag{26}$$

Note that $x^*(f_x + \delta, f_y)$ and $y^*(f_x + \delta, f_y)$ require solving $\boldsymbol{System}(f_x + \delta, f_y, s)$.

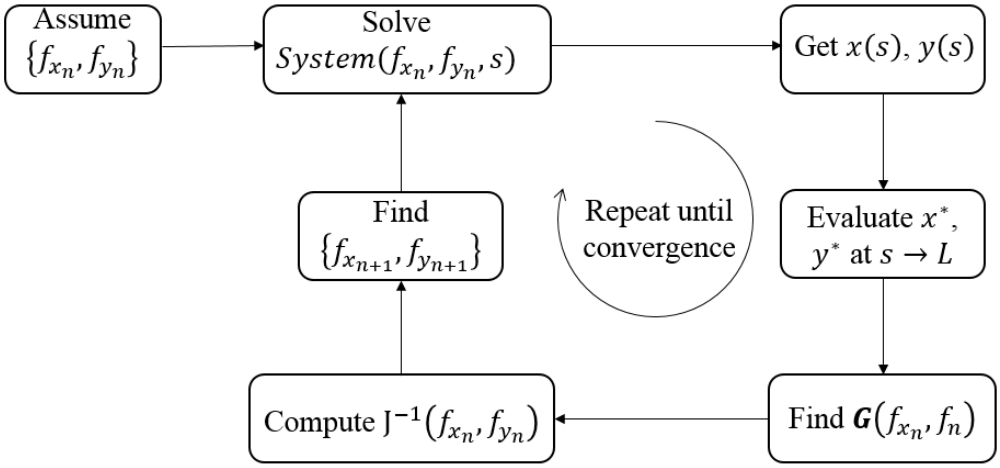

Fig. 5: Iterative approach to obtain the unknown forces f_x and f_y

V.Results and Discussions

In this section, the developed governing equations and numerical solution approach are implemented for the specific case of a tow placed on a flat surface and following a circular path. The corresponding end-point boundary conditions are first presented. Then, the results are shown for compressive and tensile regions within the tow and at different tow length. The effect of the foundation stiffness as well as the steering radius are also investigated.

A. Boundary Conditions

A steered tow-path at a constant curvature is considered for investigation. A possible arc-length parametrization for a constant curvature path (circular arc) is:

$$\boldsymbol{C}(s) = \{x(s), y(s)\} = \begin{cases} \rho \ \sin\dfrac{s}{\rho} \\ \rho\left(1 - \ \cos\dfrac{s}{\rho}\right) \end{cases}, \quad 0 \le s \le L, \tag{27}$$

where ρ is the constant radius of curvature. If we consider that $\boldsymbol{C}(s)$ is the centerline of the tow-path, then the parallel edges of the tow-path can be found by taking the parallel curves to $\boldsymbol{C}(s)$ which can be expressed as follows [9]:

$$\boldsymbol{C_p}(s) = \{x_p(s), y_p(s)\} = \begin{cases} (d+\rho)\sin\dfrac{s}{\rho} \\ \rho - (d+\rho)\cos\dfrac{s}{\rho} \end{cases}, \tag{28}$$

where d can be either a positive or a negative distance. For the case where d is positive, the parallel edge obtained by equation (28) corresponds to a path $\boldsymbol{C_p}(s)$ longer than the reference path $\boldsymbol{C}(s)$, or in other words, the tensile side of the tow. Whereas a negative value of d corresponds to the compressive edge of the tow. The enforced boundary condition at the endpoint can be obtained using the following:

$$\begin{cases} x_L = x_p(L) \\ y_L = y_p(L) + d \\ \tan\gamma_L = \dfrac{y_p'(L)}{x_p'(L)} \end{cases}. \tag{29}$$

Note that for numerical convenience, the parallel paths are shifted along the y-axis by a distance d, so that the y-coordinate of the start point corresponds to zero.

B. Results for a compressive region

In a first step to analyze the problem in hand, a worst-case scenario is considered where there is no adhesion ($k_x = k_y = 0$). Other relevant parameters such as radius of curvature, tow thickness, width and modulus for an uncured thermoset pre-impregnated tow are shown in Table 1. The shape of the deformed fibers in the compressive side of the tow are shown in Fig. 6 for different tow length ranging from 5 mm to 40 mm. For this case, half the tow width is assumed under compression, and four equal separate regions within the compressive side are analyzed. The deformed curve representing the centroid of each fiber bundle is shown in Fig. 6 using a solid line, whereas the neutral axis and the compressive edge are shown using dashed lines. The first bundle is chosen to be the closest to the neutral axis, and the remaining bundles are aligned within a distance d corresponding to 1/8th of the tow width.

At a small length, the fibers on the compressive side can absorb the differential length by the mean of compressive strains (Fig. 6, (a) and (b)), hence the fibers remain parallel to the neutral axis as intended in the design. However, at a larger length, and in the absence of adhesion, the fibers tend to deform towards the neutral axis in the form of fiber waviness (Fig. 6, (c) and (d)). This form of deformation results in fiber angle deviation from the designed angles which can be quantified directly from the solution of the tangent angle γ obtained by solving the system of equations in (20). The solution of the four unknown functions $\gamma, l', x,$ and y from that system are shown in Fig. 7 for a tow length L = 20 mm. It can be noticed from Fig. 6 (c) that the fiber bundle closest to the neutral axis remains parallel to the path. This is also reflected in the solution of the in-plane rotation γ in Fig. 7 (a): the blue line corresponding to the first bundle's tangent angle is linear (since the path has a constant curvature, the tangent angle γ is a linear function of the arc-length *s*). The remaining fiber angles deviate from the original design by ±4° as represented in Fig. 7 (a). As for the strain along the length l' shown in Fig. 7 (b), all four bundles experience compressive strains, where the bundle closest to the compressive edge experiences the most compressive strains. As for the x-coordinate shown in Fig. 7 (c), it can be noticed that *x* is a linear function of *s*, and the difference between the bundles across the tow width is negligible: this is due to the fact that the compressive strains and the rotation angle are relatively small ($1 + l' \cong 1$ and $\cos\gamma \cong 1$ thus from equation (20), $x' \cong 1$ hence $x(s) \cong s$). Lastly, the y-coordinate shown in Fig. 7 (d) indicates that the fiber bundle closest to the compressive edge undergoes the most deformation in that direction.

Table 1: Material property and geometry of the tow

$\boldsymbol{E_{11}}$	$\boldsymbol{H}$	$\boldsymbol{w}$	$\boldsymbol{\rho}$	$\boldsymbol{k_x = k_y}$
130 GPa[2]	0.184 mm	6.35 mm	0.4 m	0

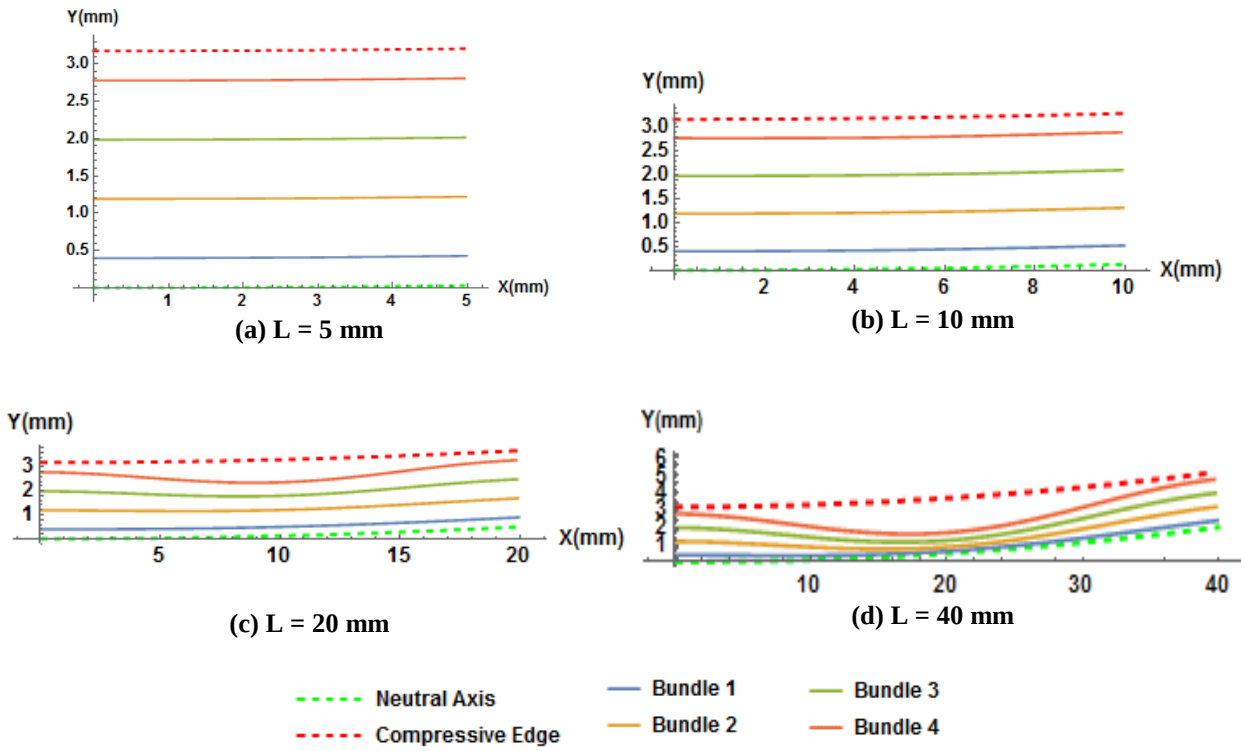

Fig. 6. Deformed fiber bundles under compression at different tow length

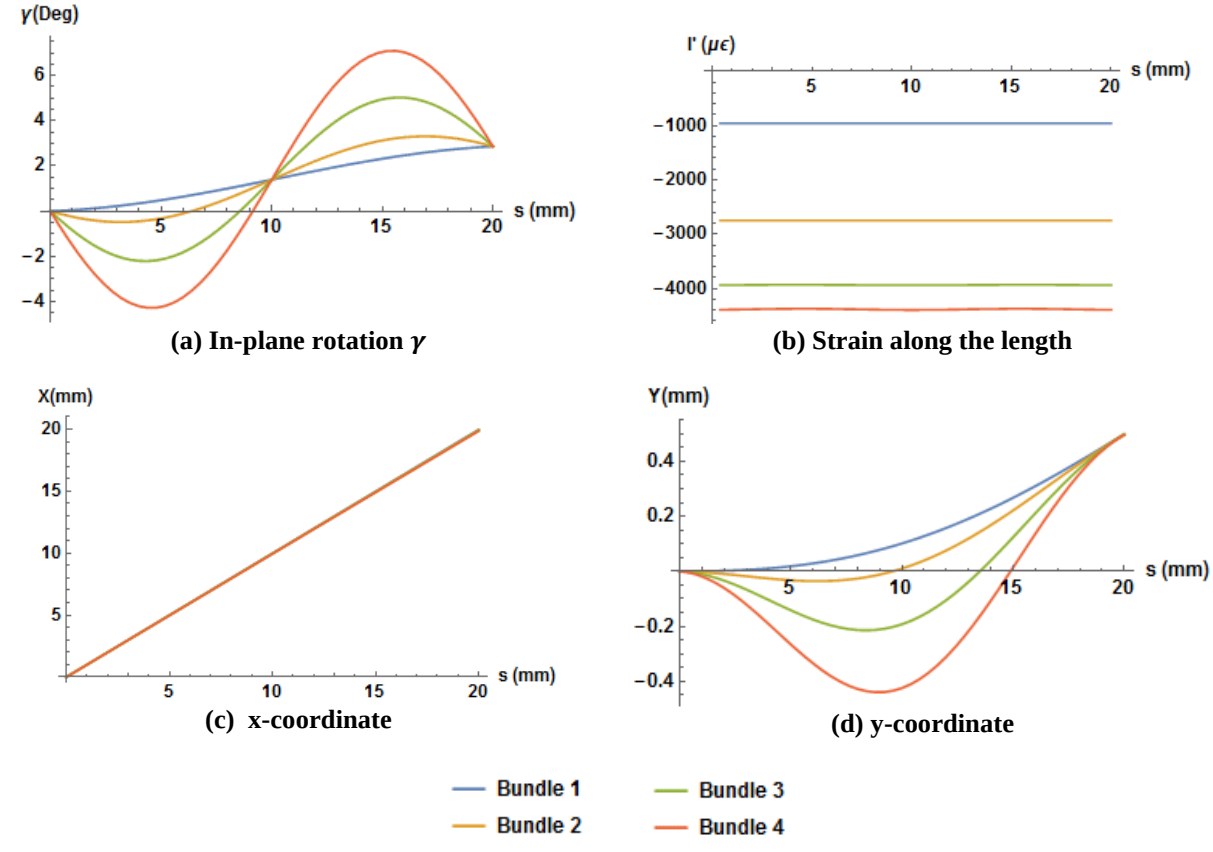

Fig. 7. Solution of equation (20) for 4 bundles under compression at L = 20 mm

C. Results for a tensile region

In this section, the analysis of fiber bundles undergoing tension within the tow is shown. Similarly to the previous section, a worst case scenario is considered when there is no adhesion between the fiber bundles and the substrate. The same material properties and tow geometry are used which can be found in Table 1. Half of the tow width is assumed to be under tension and it is divided into four separate regions for analysis. The boundary conditions corresponding to the tensile case can be obtained from equations (28) and (29) using a positive distance d. The results corresponding to the deformed shape of the fiber bundles at four different tow-lengths (L = 10 mm, 20 mm, 40 mm, and 100 mm) are shown in Fig. 8.

Similar to the compressive case, at small length, tensile strains absorb the difference in length between the path and the fiber bundles (Fig. 8 (a) and (b)). However at a larger length, the fiber bundles tend to straighten or bunch towards the centerline as shown in Fig. 8 (c) and (d). The solutions for the unknown functions of equation (20) are shown in Fig. 9 for four bundles at L = 40 mm. The fiber straightening phenomenon can be interpreted from the solution of the tangent angle γ shown in Fig. 9 (a): the fiber angle tends to be constant ($\cong 3°$) at the mid-length of the tow. This behavior is more visible for the fiber bundle closest to the tensile edge. In addition to the fiber bunching, tensile strains are still a significant mode of deformation as shown in Fig. 9 (b) where the fiber bundle closest to the tensile edge experiences the most strain. Similar to the previous section, the results for the x-coordinates show a linear relationship between the x-coordinate and the arc-length. Finally, the results for the y-coordinate in Fig. 9 (d) show the bunching/ straightening deformation mode of the fiber bundles.

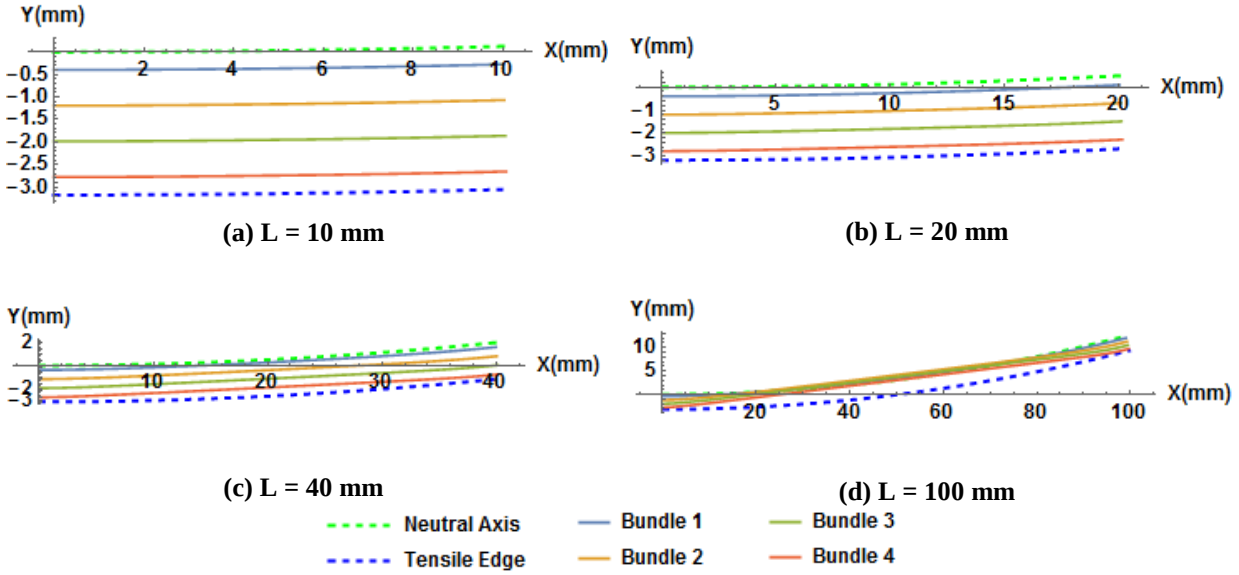

(a) L = 10 mm **(b) L = 20 mm**

(c) L = 40 mm **(d) L = 100 mm**

Fig. 8. Deformed fiber bundles under tension at different tow length

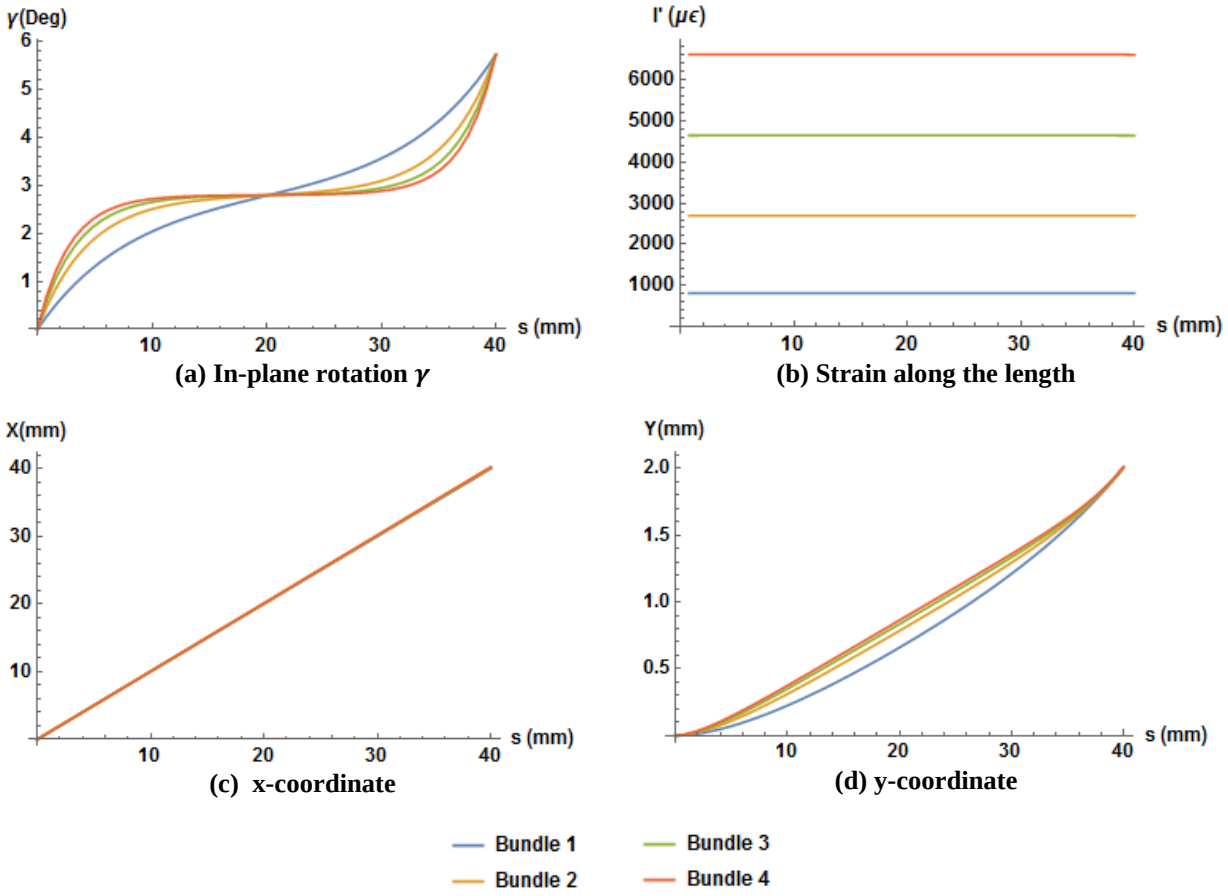

Fig. 9. Solution of equation (20) for 4 bundles under tension at L = 40 mm

D. Effect of the foundation's stiffness

In this set of results the effect of the stiffness foundation on the deformed shape of the fibers is investigated. A reasonable assumption can be made where the foundation is isotropic having similar values in the x and y-directions. Other material properties and tow geometry are shown in Table 2. In this case, the length of the tow section, as well as the steering radius are kept constant, whereas the value of the foundation stiffness is varied between 0 and 10^{10} N/m^2. The tow is assumed to be under pure bending: half of the tow is under tension and the other half is under compression. Five equal separate region are considered for the analysis, where two of them represent the fiber bundles under tension, two for the compression, and one coincides with the neutral axis. An example of the deformed fiber bundles with $k = 10^6\ N/m^2$ is shown in Fig. 10: bundle 1 and 2 are under tension, bundle 3 coincides with the neutral axis, and bundles 4 and 5 are under compression and undergo some fiber waviness.

Table 2: Material property and geometry of the tow

E_{11}	H	w	L	ρ
130 GPa	0.184 mm	6.35 mm	30 mm	0.4 m

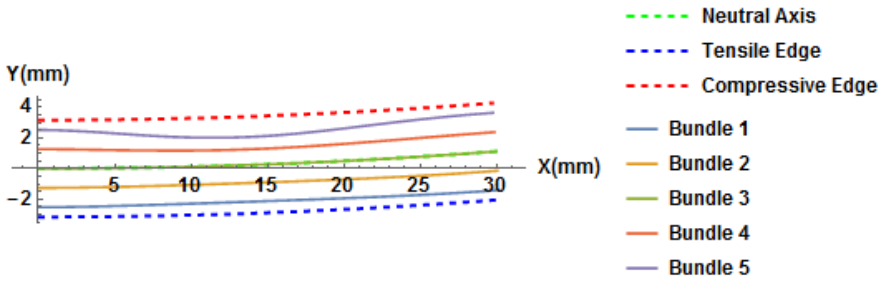

Fig. 10: Deformed fiber bundles for $k = 10^6\ N/m^2$

To quantify the effect of the foundation's stiffness on the deformation of the fiber bundles, the displacement in the transverse direction to the fibers $u_r(s)$ is considered (Fig. 4). $u_r(s)$ can be computed from the displacements in the x- and y-directions $u(s)$ and $v(s)$ using:

$$u_r(s) = v(s)\cos\gamma(s) - u(s)\sin\gamma(s)\,. \tag{30}$$

A zero value for u_r means that the fiber bundle remains in the same location as placed by the AFP machine head. The maximum value of the u_r (in absolute value) for the five different fiber bundles is shown in Fig. 11 for different values of the foundation's stiffness (logarithmic scale). Large values of k ($k > 10^7\ N/m^2$) result in almost zero displacement in the transverse direction: this means that the foundation is stiff enough to hold the fibers in their intended location. For small values of k ($k < 10^6\ N/m^2$), the displacement in the transverse direction is constant and does not change from the value of $k = 0$. This indicates that the foundation is very weak and unable to resist other deformation modes. Finally, there is an intermediate phase where k is between $10^6\ N/m^2$ and $10^7\ N/m^2$ during which the fiber bundles experience a slight increase in the displacement and then a sudden drop. In this phase, all energy terms are equally important in the governing equations resulting in a highly nonlinear system. The slight increase in the displacement is due to the fact that the waviness and bunching are not evenly distributed throughout the whole length anymore, but they are localized in one section of the tow. It is also worth to mention that fiber straightening on the tensile side of the tow is not as severe as the fiber waviness on the compressive side: the maximum displacement for bundles 1 and 2 is much smaller than the one for bundles 4 and 5. Note that the fiber bundle coinciding with the neutral axis does not experience any displacement in the transverse direction and remains in its intended location.

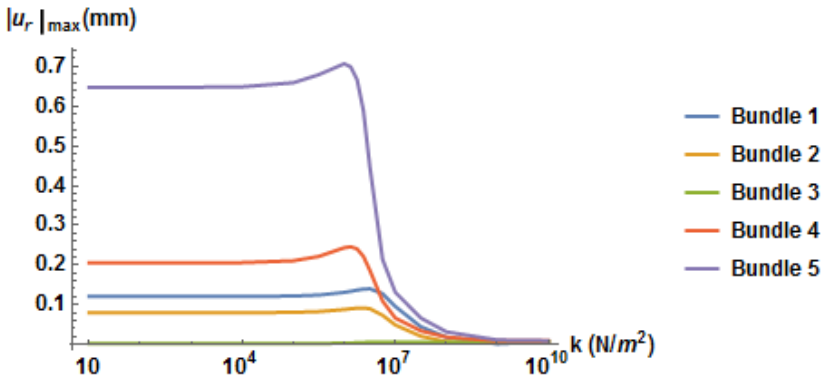

Fig. 11: Effect of the foundation stiffness on the displacement in the transverse direction

E. Effect of the steering radius

In this section the effect of the steering radius is investigated. The same tow properties provided in Table 2 are considered in this section while varying the steering radius. The tow is assumed to be under pure bending, and it is divided into five sections: two under tension (bundle 1 and 2), two under compression (bundle 4 and 5), and one coinciding with the neutral axis (bundle 3). Similar to the previous section, the maximum (absolute value) of the displacement in the transverse direction is monitored as a function of the steering radius for two values of the foundation's stiffness: $k = 0$ and $10^7\ N/m^2$. The results are shown in Fig. 12 and Fig. 13 respectively. It can be observed that increasing the steering radius decreases the displacement of the fiber bundles in the transverse. This is

predictable since a smaller steering radius of curvature means a larger difference in length between the fiber and the path. For the first case (worst case scenario) where the stiffness of the foundation is zero, a minimum steering radius of 1.5 m is required for a significantly small u_r. However, for the case where $k = 10^7\ N/m^2$, only small radii of curvature $\rho < 0.5$ m lead to a significant displacement of the fiber bundles in the transverse direction.

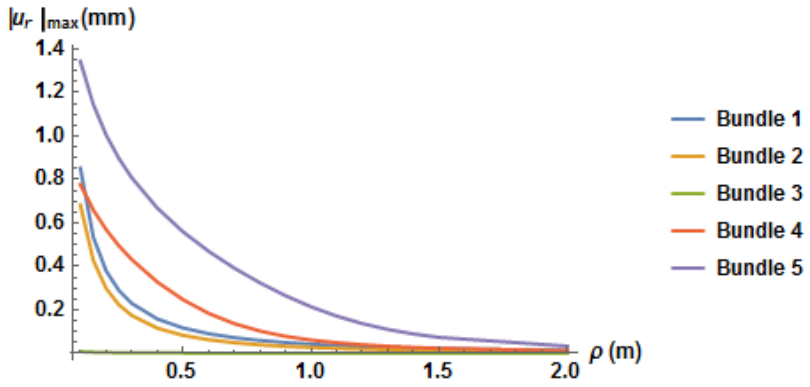

Fig. 12: Effect of the steering radius on the displacement in the transverse direction for $k = 0$

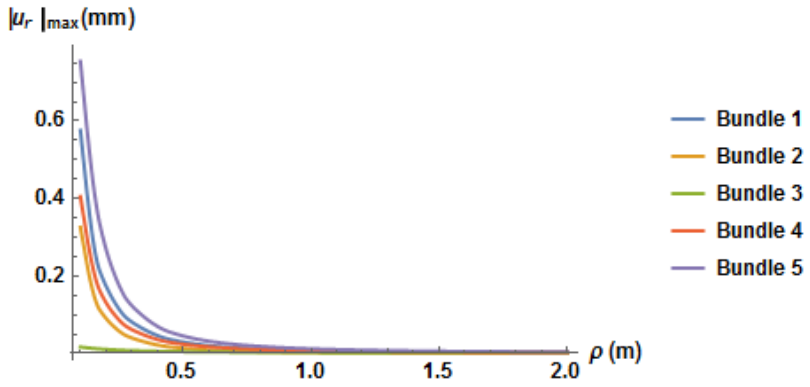

Fig. 13: Effect of the steering radius on the displacement in the transverse direction for $k = 10^7\ N/m^2$

VI. Conclusion and Future Work

During the AFP process, steering is necessary to manufacture curved shells and variable stiffness plates. Several tow deformation mechanisms due to steering are proposed in this work and classified as strain deformation (compressive, tensile, and shear), in-plane deformations (waviness and bunching), and out-of-plane deformations (wrinkling and folding). The focus of this paper is to understand the formation of the in-plane ones, and to determine the final shape of the deformed tow based on set of material properties and process parameters. A novel approach is presented based on the physics of a constrained path, where the fiber tow is modeled as several fiber bundles laying on a stiff foundation. The total energy is derived based on the contribution of the strain energy, work, and energy stored in elastic foundation for the case of small strains and large rotations. The total energy of the system is then minimized, and the governing differential equations are generated using Euler-Lagrange principle. A novel numerical method is implemented to solve the differential equations and the integral boundary constraints. This method is applied to path steered at constant curvature (circular arc). The dominant deformation mechanism is determined based on the material properties and process parameters such as length, thickness, width, curvature, longitudinal bundle stiffness, and the stiffness of the foundation. Results show that at a small length during the additive process, strain deformation are dominant for the tensile and compressive areas within the tow. At larger length, fiber waviness occurs on the

compressive side of the tow, whereas fiber bunching/straightening occurs on the tensile side of the tow. Increasing the stiffness of the foundation can reduce the in-plane deformation of the tow and possibly eliminating it for a very stiff foundation. However, steering tow at smaller radii of curvature increases the magnitude of the in-plane deformation mechanisms.

Future work will consist of investigating the out-of-plane deformation mechanisms, and examining the importance of other parameters such as shear and transverse strain. Experimental work is necessary to determine the values of the stiffness of the foundation and to relate it to other process parameters such as speed and layup temperature.

VII. Acknowledgments

The authors would like to thank The Boeing Company for their support of this work. Also, the authors would like to thank Dr. Brian Tatting for the invaluable comments and suggestions.

References

[1] Lukaszewicz, D. H. J. A., Ward, C., and Potter, K. D., "The engineering aspects of automated prepreg layup: History, present and future," *Composites Part B: Engineering*, vol. 43, 2012, pp. 997–1009.

[2] Beakou, A., Cano, M., Le Cam, J. B., and Verney, V., "Modelling slit tape buckling during automated prepreg manufacturing: A local approach," *Composite Structures*, vol. 93, 2011, pp. 2628–2635.

[3] Matveev, M. Y., Schubel, P. J., Long, A. C., and Jones, I. A., "Understanding the buckling behaviour of steered tows in Automated Dry Fibre Placement (ADFP)," *Composites Part A: Applied Science and Manufacturing*, vol. 90, 2016, pp. 451–456.

[4] Wehbe, R., "Modeling of Tow Wrinkling in Automated Fiber Placement based on Geometrical Considerations," University of South Carolina, 2017.

[5] Wehbe, R., Tatting, B. F., Harik, R., Gurdal, Z., and Miller, E., "Geometrical Modeling of Tow Wrinkles in Automated Fiber Placement," *Submitted to CAD Computer Aided Design*.

[6] Hormann, P. M., *Thermoset automated fibre placement - on steering effects and their prediction*, 2015.

[7] Kassapoglou, C., *Design and Analysis of Composite Structures*, WILEY, 2013.

[8] Timoshenko, S. P., and Gere, J. M., *Theory of Elastic Stability*, Dover Publications, 1961.

[9] Rousseau, G., Wehbe, R., Halbritter, J., and Harik, R., "Automated Fiber Placement Path Planning: A State-of-the-art review," *Computer-Aided Design and Application*, vol. 16, 2019, pp. 172–203.